Application of density functional theory to tethered polymer chains: Athermal systems

ARTICLE *in* THE JOURNAL OF CHEMICAL PHYSICS · AUGUST 2002

Impact Factor: 2.95 · DOI: 10.1063/1.1491242

3 AUTHORS, INCLUDING:

John Mccoy
New Mexico Institute of Mining and Technology
114 PUBLICATIONS **2,054** CITATIONS

Application of density functional theory to tethered polymer chains: Athermal systems

John D. McCoy[a] and Yuan Ye
Department of Materials and Metallurgical Engineering, New Mexico Institute of Mining and Technology, Socorro, New Mexico 87801

John G. Curro
Sandia National Laboratories, Albuquerque, New Mexico 87185

(Received 19 February 2002; accepted 14 May 2002)

Athermal, tethered chains are modeled with density functional (DFT) theory for both the explicit solvent and continuum solvent cases. The structure of DFT is shown to reduce to self-consistent-field theory in the incompressible limit where there is symmetry between solvent and monomer, and to single-chain-mean-field (SCMF) theory in the continuum solvent limit. We show that by careful selection of the reference and ideal systems in DFT theory, self-consistent numerical solutions can be obtained, thereby avoiding the single chain Monte Carlo simulation in SCMF theory. On long length scales, excellent agreement is seen between the simplified DFT theory and molecular dynamics simulations of both continuum solvents and explicit-molecule solvents. In order to describe the structure of the polymer and solvent near the surface it is necessary to include compressibility effects and the nonlocality of the field. © *2002 American Institute of Physics.*
[DOI: 10.1063/1.1491242]

I. INTRODUCTION

Polymer chains tethered to a surface provide solutions to a number of technologically important problems. Such applications include the synthesis of biocompatible materials, control of protein adsorption, stabilization of colloids, and the modification of surfaces to control hydrophobicity. These are applications where the chains are in the presence of solvents, or ''wet-brushes.'' The ''dry-brush,'' or solventless, case is most applicable as a controlled adhesive. Moreover, wet-brushes are commonly analyzed in the dried state with, for instance, atomic force microscopy (AFM). Consequently, it is useful to understand not only the structure of the wet and of the dry brush states individually, but also the relationship between the two.

The purpose of the present investigation is to develop a theory to model the equilibrium structure and properties of tethered polymer layers in the vicinity of the surface. This problem has been studied extensively by many workers in the past. Scaling approaches, where the polymer profile is assumed to be a step function, were developed by Alexander[1] and de Gennes.[2] Self-consistent field (SCF) theories were developed and numerically implemented by a number of workers.[3–8] Milner and co-workers[9] were able to obtain an analytical solution to the SCF problem under certain conditions that leads to a parabolic density profile for the polymer. A related approach, the single chain mean field (SCMF) theory, was developed by Carignano and Szleifer[10] in a manner that, in effect, incorporates a single chain Monte Carlo simulation as part of a self-consistent field theory. The reader is referred to several reviews on tethered polymer chains that have appeared in the recent literature.[11–13] Computer simulations of tethered chains by Grest and Murat[14–18] and by Lai and Binder[19] have provided valuable insights and made it possible to evaluate the accuracy of the various theories.

Unlike the previous work on this problem, here we develop the theory using classical density functional theory (DFT). Classical DFT approaches the problem of classical particles in an anisotropic environment from a more general perspective than SCF. Density functional theory was first applied to molecular liquids by Chandler, McCoy, and Singer[20] and subsequently applied to free polymers near surfaces.[21–24] It is worthwhile to reformulate the tethered chain problem within the context of DFT not only because of the theory's generality, but also because doing so illuminates the various approximations that are necessary to recover conventional SCF theories.

We will, first, apply DFT theory to the case of tethered polymer chains in a continuum solvent, a problem studied extensively both by Murat and Grest[15–18] and by Lai and Binder[19] with MD simulation. Carignano and Szleifer[10] obtained excellent agreement with the Murat and Grest simulations with their SCMF theory. As will be shown later, in the appropriate limit our DFT theory gives comparable results to the SCMF approach. However, in our implementation of DFT we are able to obtain solutions numerically, thereby avoiding a Monte Carlo simulation.

Second, we apply our DFT approach to the problem of tethered chains in the presence of an explicit solvent and compare with corresponding MD simulations.[17] To our knowledge, this is the first time quantitative comparisons have been made between theory and simulation for this problem. This application serves to highlight a significant advantage of our DFT approach which is that it points the way

[a]Author to whom correspondence should be addressed.

toward making improvements in SCF theory.

In this paper we present the details of the DFT application to tethered chains in Appendices A and B. In the theory section we discuss the approximations necessary to make contact with SCF and SCMF theories. We also demonstrate that the theory can be implemented in a manner that allows us to obtain numerical solutions. Later we show results comparing our DFT theory with MD simulations, both in continuum and explicit solvents.

II. THEORY

Since both SCF (Refs. 1–9) and DFT (Refs. 20–24) theories are, generically, self-consistent-field theories, the specific approximations which distinguish the meaning of the term ''SCF theory'' from the broader ''DFT theory'' are largely determined by colloquial usage in the literature. The two approximations that usually distinguish SCF theory are as follows. First, the only explicit length scale in the problem is assumed to be the radius of gyration. This means that all interactions between sites are ''local'' (i.e., delta functions), and that the chains are ''Gaussian Threads'' which can be described by a differential equation. Second, the only effect of the repulsive part of the inter-molecular interactions is assumed to be the enforcement of incompressibility. Consequently, incompressibility is constrained in SCF through an undetermined multiplier and repulsive (or excluded volume) interactions are subsequently ignored. As a result, for the tethered chain problem, the only parameters in the SCF calculation are the chain length, N; the Flory–Huggins χ-parameter; and the surface coverage, ρ_A. One expects that such calculations would be accurate on long length scales, but would fail to capture short range, local packing effects. In the current study, we make some, but not all, of the approximations of SCF theory.

The solution method for the density profile of the tethered chains is essentially that of Ref. 21. The total site density, $\rho(z)$, at a distance z from the wall can be computed from the coupled functional equations,

$$\begin{aligned}\rho(z) &= F[U^0(z)],\\ U^0(z) &= G[\rho(z)],\end{aligned} \tag{2.1}$$

where $U^0(z)$ is an external field whose purpose is to mimic the effects of the solvent and of the other chains on a given tethered chain. The specific development of the forms of these relationships from a free energy functional is detailed in the Appendices.

A. The ideal and reference systems

The definition and careful manipulation of the ideal system are central to the successful application of DFT to polymeric systems. The importance of the ideal system is clearly shown in the first of Eqs. (2.1) which represents the computation of the density profile of a single tethered chain (i.e., the ideal system) in an external field $U^0(z)$; this is the subject of Appendix A. The term ''ideal chain'' in DFT theory refers to a polymer chain that does not interact explicitly with the other chains in the system. However, depending on the specific choice of the ideal chain, it may or may not interact with itself via, for example, excluded volume interactions. Even though SCF and DFT theories reduce the many chain problem to the considerably simpler, single ideal chain problem, this simpler problem still cannot be solved in closed form in the presence of an external field. Since a freely-jointed-chain, or random walk model, is Markovian, we can calculate the density distribution in the external field for this model numerically, for example by using the Fourier transform technique described in Appendix A. By contrast, in the SCMF theory of Szleifer and co-workers[10] on tethered chains, and in our earlier work on free chains,[22,23] the ideal chain problem was solved with intra-molecular excluded volume interactions between chain segments. In order to compute the density distribution for this self-avoiding walk (SAW) model, these workers required Monte Carlo techniques as part of their self-consistent field calculation. In both ideal chain models, the two equations in Eq. (2.1) are solved iteratively until a self-consistent density profile and external field are obtained. Later in this paper we will demonstrate that equivalent results can be obtained from either the random walk or SAW model as the choice for the ideal system.

In order to see the importance of the ideal system more clearly, let us consider the problem of interest in more detail—that is, tethered polymer chains whose segments are a distance z from the tethering surface. The external field $U^0(z)=G[\rho(z)]$ acts on a single tethered chain, the ideal chain, in order to mimic the effects of the other chains in the system in a mean field sense. The form of this field can be found by minimizing the grand potential free energy with respect to the inhomogeneous density profile $\rho(z)$. The algebraic details of this procedure are reviewed in Appendix B and leads to Eq. (B11) that can be rearranged as follows for the polymer and solvent fields:

$$\begin{aligned}U_p^0(r) &= U_p(r) - c_{p,s} * \Delta\rho_s(r)\\ &\quad + [(\omega^{-1} - \omega_0^{-1}) - \rho_{p,\mathrm{ref}} c_{p,p}] * \frac{\Delta\rho_p(r)}{\rho_{p,\mathrm{ref}}},\end{aligned}$$

$$U_s^0(r) = U_s(r) - c_{s,s} * \Delta\rho_s(r) - c_{s,p} * \Delta\rho_p(r), \tag{2.2}$$

where $c_{i,j}(r)$ is the intermolecular direct correlation function between sites of type p (polymer) or s (solvent). The quantity $\omega^{-1}(r)$ is the functional inverse of the intramolecular correlation function of the fully interacting polymer chains, and $\omega_0^{-1}(r)$ is the corresponding inverse for the ideal chain. The direct correlation functions in Eq. (2.2) are to be evaluated in the homogeneous reference state of density $\rho_{p,\mathrm{ref}}$. In Eq. (2.2), ''$*$'' denotes the convolution integral $f*g(r) = \int f(\underline{r}-\underline{r}')g(\underline{r}')d\underline{r}'$. The function $U(r)$ is the bare external field on the fully interacting, inhomogeneous system due to the presence of the surface; the difference $\Delta\rho(r)$ is $\rho(r) - \rho_{\mathrm{ref}}$ and $\rho(r)$ is the density profile of the inhomogeneous system. In Eq. (2.2), constant terms in $U^0(r)$ have been dropped since the density profile is sensitive only to differences in the external field. On the other hand, the free energy does depend upon constant offsets in the potentials, and

some care must be taken when treating phase transitions where the value of the free energy (and not only the location of its minimum) is of importance.[22]

Two choices need to be made at this point for the ''ideal'' and ''reference'' systems. The ideal system can be chosen to be either a random walk or a self-avoiding, random walk (SAW) chain. Since the random walk model can be treated numerically, whereas a SAW model requires a simulation, the choice of a random walk model as the ideal system is highly desirable. Whether or not this is a suitable choice is closely tied to the second choice that must be made; that of the reference system.

The reference system is the homogeneous state about which the Helmholtz free energy of the inhomogeneous system is expanded in Eq. (B6). Commonly, the bulk liquid in equilibrium with the inhomogeneous system is selected as the reference state. This is a reasonable choice for systems such as untethered chains in a pore that are clearly in equilibrium with a bulk liquid reservoir. It is important to recognize, however, that the choice of the reference state is arbitrary to a degree. In the case of chains tethered to a surface, the system far from the wall (which the tethered chains are in equilibrium with) consists of a pure solvent; a problematic choice for the reference system. In particular, the division by $\rho_{p,\mathrm{ref}}$ in Eq. (2.2) makes the bracketed term diverge when $\rho_{p,\mathrm{ref}}=0$ unless, of course, $\omega(r)=\omega^0(r)$. Consequently, for this choice of reference system, a SAW ideal chain is required for the accurate portrayal of the single chain structure factor of a dilute solution of a polymer in a good solvent in order to avoid the divergence of the field in Eq. (2.2). This was the approach taken in the SCMF theory.

Rather than taking the reference system to be the far-field, polymer density, which is zero, we instead choose the $\rho_{p,\mathrm{ref}}$ to be the average density within the polymer layer. It is physically reasonable that the density in the region where the polymer is actually present should determine the physics of the system. This can be achieved by using a ''mass weighted'' average of the density defined as

$$\rho_{p,\mathrm{ref}}=\langle\rho\rangle=\frac{\int_0^H\rho^2(z)dz}{\int_0^H\rho(z)dz}, \tag{2.3}$$

which is appropriate for the one-dimensional density profile and field assumed in this work. Note that the ''number weighted'' average would be zero due to the large volume of solvent far from the surface. For this reference system, $\rho_{p,\mathrm{ref}}$ is no longer zero and the bracketed term in Eq. (2.2) is not dominated by $(\omega^{-1}-\omega_0^{-1})$ but is controlled by the $c(r)$ term. For sufficiently high surface coverages, ρ_A, such that $\langle\rho\rangle$ is larger than a particular threshold density, ρ^*, our reference system corresponds to a uniform polymer solution in the concentrated or semidilute regime. This crossover density from dilute to semidilute solutions is defined by

$$\rho^*\sigma^3\sim\frac{3N\sigma^3}{4\pi R_g^3}\sim\frac{3.5}{N^{3\nu-1}}, \tag{2.4}$$

where $R_g\approx\sigma N^{\nu}/\sqrt{6}$ and ν is the Flory exponent. Hence, a reasonable choice for the ideal chain consistent with this reference system would be random walk chain with no excluded volume ($\nu=1/2$).

As we proceed to still lower surface coverages, the theory is affected by a second threshold density, the crossover surface coverage, ρ_A^*, from the brush to the ''mushroom'' regime where the tethered chains no longer overlap with each other,

$$\rho_A^*\sigma^2=\frac{\sigma^2}{\pi R_g^2}=\frac{6}{\pi}N^{-2\nu}. \tag{2.5}$$

As long as $\rho_A>\rho_A^*$ we expect our assumption of a one-dimensional field and profile to be valid. However it is possible that $\langle\rho\rangle<\rho^*$ while $\rho_A>\rho_A^*$. When this occurs, we take our reference system to be $\rho_{p,\mathrm{ref}}=\rho^*$. Since our reference system is still in the semidilute regime, we can still choose our ideal system to be a random walk chain. At surface coverages below ρ_A^* the tethered chains become isolated, and the tethered layer can no longer be described by a one-dimensional field. In this regime, it would be necessary to treat the fields and profiles in a two-dimensional generalization of the theory, in a manner similar to the approach of Balazs and co-workers.[25]

Thus, it can be seen that our choice of reference system such that $\rho_{p,\mathrm{ref}}\geqslant\rho^*$ allows us to take our ideal chain to be a random walk model. Consequently the term $(\omega^{-1}-\omega_0^{-1})$ can be safely ignored and the bracketed term in Eq. (2.2) is essentially controlled by the direct correlation function $c_{pp}(r)$. This choice of the reference and ideal systems is very beneficial from a computational standpoint since the density profile calculation in Eq. (2.1) can be performed without resorting to a simulation.

B. The connection between SCF and DFT theories

At this point, various simplifying approximations in the spirit of SCF theory can be made. First, the length scale associated with $c(r)$ is assumed to be negligible, and $c(r)$ is treated as a delta function, $c(r)=\hat{c}(0)\delta(r)$. For our choice of ideal and reference systems, this locality approximation leads to

$$\begin{aligned}U_p^0(r)&=U_p(r)-\hat{c}_p^+(0)\Delta\rho^+(r)-\hat{c}_p^-(0)\Delta\rho^-(r),\\ U_s^0(r)&=U_s(r)-\hat{c}_s^+(0)\Delta\rho^+(r)-\hat{c}_s^-(0)\Delta\rho^-(r),\end{aligned} \tag{2.6}$$

where we introduce the following variable definitions:

$$\hat{c}_p^+(0)=(\hat{c}_{pp}(0)+\hat{c}_{ps}(0))/2;$$

$$\hat{c}_s^+(0)=(\hat{c}_{ss}(0)+\hat{c}_{ps}(0))/2;$$

$$\hat{c}_p^-(0)=(\hat{c}_{pp}(0)-\hat{c}_{ps}(0))/2;$$

$$\hat{c}_s^-(0)=(\hat{c}_{ps}(0)-\hat{c}_{ss}(0))/2;$$

$$\rho^+=\rho_p+\rho_s;\quad \rho^-=\rho_p-\rho_s.$$

The $\hat{c}(0)$ is conveniently viewed as the sum of a contribution due to the attractive site–site interactions, $\hat{c}^A(0)>0$ and one due to the repulsive interactions, $\hat{c}^R(0)<0$. Since it is usually the case that $|\hat{c}^R(0)|\gg|\hat{c}^A(0)|$, the $\hat{c}^+(0)$ are dominated by the $\hat{c}^R(0)$'s. These terms serve as a restoring force such

that for large (negative) $\hat{c}^+(0)$'s, one finds that $\Delta\rho^+(r) \sim 0$. Consequently, it is often expedient to include an undetermined multiplier term of the form $\int\lambda(r)\Delta\rho^+(r)dr$ in ΔW in Eq. (B9) to constrain the system so that $(\rho_p+\rho_s)$ is a constant. When this constraint is enforced through $\delta W/\delta\lambda = \delta W/\delta\rho = \delta W/\delta U^0 = 0$, the expression for the fields becomes

$$U_p^0(r) = U_p(r) - 2\hat{c}_p^-(0)\rho_p(r) + \lambda(r),$$
$$U_s^0(r) = U_s(r) - 2\hat{c}_s^-(0)\rho_p(r) + \lambda(r), \tag{2.7}$$

where additional constant terms have been omitted. By splitting the $\hat{c}^-(0)$'s into repulsive and attractive contributions. The fields can now be written as

$$U_p^0(r) = U_p(r) - \xi_p\rho_p(r) - 2\chi_p\phi(r) + \lambda(r),$$
$$U_s^0(r) = U_s(r) + \xi_s\rho_p(r) + 2\chi_s\phi(r) + \lambda(r), \tag{2.8}$$

where

$$\xi_p = (\hat{c}_{pp}^R(0) - \hat{c}_{ps}^R(0)); \quad \xi_s = (\hat{c}_{ss}^R(0) - \hat{c}_{ps}^R(0));$$
$$\chi_p = \frac{\rho_{\text{tot}}}{2}(\hat{c}_{pp}^A - \hat{c}_{ps}^A); \quad \chi_s = \frac{\rho_{\text{tot}}}{2}(\hat{c}_{ss}^A - \hat{c}_{ps}^A); \tag{2.9}$$

$\phi(r) = \rho_p(r)/\rho_{\text{tot}}$; and $\rho_{\text{tot}} = \rho_p + \rho_s$. The χ's are related[22] to the Flory–Huggins χ-parameter through $\chi = \chi_p + \chi_s$. In addition, by making the symmetry assumptions that $\chi_p = \chi_s$, and that $\xi_p = \xi_s = 0$ in the spirit of Flory–Huggins theory, we are led to the well known field commonly employed in standard SCF theory,

$$U_p^0(r) = U_p(r) - \chi\phi(r) + \lambda(r),$$
$$U_s^0(r) = U_s(r) + \chi\phi(r) + \lambda(r). \tag{2.10}$$

Of course, $\xi_p = \xi_s = 0$ does not rigorously hold when there is asymmetry between monomeric and solvent structure. This effect is extreme for the case of athermal polymer brushes, where there is no solvent, or in a model where the solvent is treated as a continuum existing solely to make up the difference between ρ_p and ρ_{tot}. This is precisely the system studied in the MD simulations of Murat and Grest.[15–18] Since the solvent molecules are not explicitly considered, the direct correlation functions associated with the solvent are zero resulting in $\xi_p = \hat{c}_{pp}^R(0;\langle\rho\rangle)$ and $\xi_s = 0$. Thus, in our approach for the continuum solvent case, the fields become

$$U_p^0(r) = U_p(r) - \hat{c}_{pp}^R(0;\langle\rho\rangle)\rho_p(r) - \chi\phi(r) + \lambda(r),$$
$$U_s^0(r) = U_s(r) + \chi\phi(r) + \lambda(r), \tag{2.11}$$

where the density of the reference system $\rho_{p,\text{ref}} = \langle\rho\rangle$ is explicitly denoted. In the SCMF theory, $\langle\rho\rangle$ would be 0 while, in the current study, $\langle\rho\rangle$ is determined through the average in Eq. (2.3). In the present investigation, we consider only the athermal solution where $\chi = 0$. We will study both the compressible, continuum solvent where $\lambda(r) = 0$, as well as, the incompressible limit where the Langrange multiplier $\lambda(r) \neq 0$ enforces the incompressibility constraint of $\rho_{\text{tot}}\sigma^3 = 1$. Since we are dealing with tangent, hard-site chains, the $\hat{c}_{p,p}^R(0)$ can be found[21] from the equation of state for the bulk polymer of density $\langle\rho\rangle$. Finally, in order to model athermal, tethered chains in the presence of an explicit solvent, we take $\xi_p = \xi_s = 0$ with incompressibility enforced.

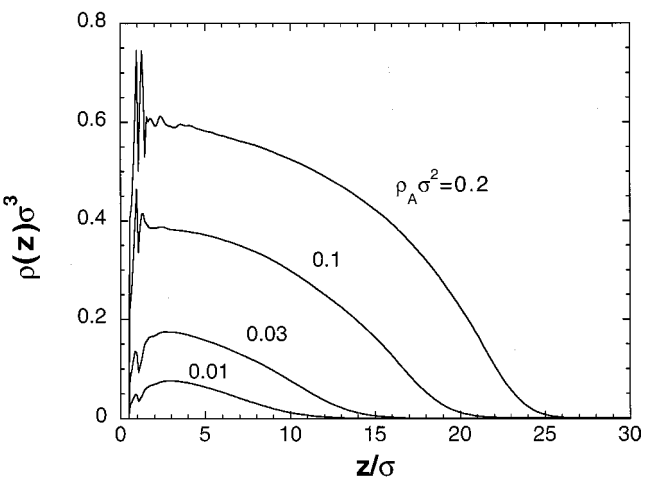

FIG. 1. Conventional SCF (with finite extensibility) results for ideal chains for $N = 50$. Surface coverages of $\rho_A\sigma^2 = 0.01$, 0.03, 0.1, 0.2.

III. RESULTS AND DISCUSSION

To provide a basis of comparison with previous work we first treat our model with conventional SCF theory in the athermal limit for which the polymer and solvent fields in Eq. (2.10) reduce to

$$U_p^0(z) = U_p(z) + \lambda(z),$$
$$U_s^0(z) = U_s(z) + \lambda(z). \tag{3.1}$$

It can be seen from this equation that the only molecular content left in these fields is the Lagrange multiplier $\lambda(z)$ that enforces the incompressibility constraint. These fields were used to solve for the density profiles of $N = 50$ unit tethered chains with surface coverages (chains/area), $\rho_A\sigma^2$, of 0.01, 0.03, 0.10, and 0.20, and of $N = 100$ chains for $\rho_A\sigma^2$ of 0.03 and 0.07. As discussed earlier, our calculations were performed with a random-walk, ideal chain in the external field using the Fourier transform method discussed in Appendix A, where 300 Fourier components were used for the $N = 50$ chains and 600 components, for the $N = 100$ chains. The results, which would be applicable to athermal, wet brushes are shown in Fig. 1. Although the chains become strongly stretched for the two largest ρ_A's, it can be seen that the profiles are well described by parabolas. These are in good qualitative agreement with previous SCF results;[9] however, since most of the literature results are lattice calculations without finite extensibility, direct comparison is difficult.

In order to test the accuracy of our approach we will first make contact with the continuum solvent, MD simulations of Murat and Grest[14–18] who considered bead–spring model chains tethered to a hard wall for a range of surface coverages. No solvent molecules were explicitly treated in most of their simulations. Instead, solvent-induced, intramolecular attractions were introduced to mimic the effects of solvent quality. Here we will focus on the athermal simulations, cor-

responding to good solvent conditions. In our theory this implies that $\chi_p=\chi_s=0$ in the equations developed in the previous section.

The appropriate fields to use in this case are depicted in Eq. (2.11) which, in the athermal limit, reduce to

$$U_p^0(r)=U_p(r)-\hat{c}_{pp}^R(0;\langle\rho\rangle)\rho_p(r)+\lambda(r),$$
$$U_s^0(r)=U_s(r)+\lambda(r). \tag{3.2}$$

Note the presence of the extra term in the polymer field that arises when the direct correlation function, $\hat{c}_{ps}^R(0)$, vanishes as a result of the lack of solvent interactions in the system. We employed the polymer and solvent fields in Eq. (3.2) in two types of DFT calculations using the ideal and reference systems discussed earlier. In one case we envision the presence of ideal, gaslike solvent molecules whose only purpose is to ensure that $\rho_p(z)+\rho_s(z)=$constant. This incompressibility constraint is enforced through the Lagrange multiplier $\lambda(z)$. The other case we consider more closely matches the simulation where no solvent molecules are present. This corresponds to putting $\lambda=0$ in Eqs. (3.2) thereby allowing the system to be compressible.

In this investigation, we evaluated the polymer/polymer direct correlation function $\hat{c}_{pp}^R(0,\langle\rho\rangle)$ in Eq. (3.2) from the equation-of-state of a bead–spring polymer melt having a density of $\langle\rho\rangle$ corresponding to our reference state. The zero-wave-vector, direct-correlation function can be related to the isothermal compressibility $\kappa_T=-(\partial \ln V/\partial P)_T$ according to[21]

$$\langle\rho\rangle\hat{C}_{pp}(0,\langle\rho\rangle)=\frac{1}{N}-\frac{1}{\langle\rho\rangle k_BT\kappa_T}. \tag{3.3}$$

The compressibility, and, hence, the direct correlation function, was obtained at each density from simulation data[26] for repulsive bead-spring chain melts and fit[21] to a Carnahan and Starling form,

$$\frac{P}{\langle\rho\rangle k_BT}=\frac{1}{N}+\frac{K_1\eta+K_2\eta^2+K_3\eta^3+K_4\eta^4}{(1-\eta)^3}, \tag{3.4}$$

where the packing fraction is $\eta=\pi\langle\rho\rangle/6$, and the coefficients, K_i, have a molecular weight dependence[21] given by

$$K_1=4-2X-1.248X^2,$$
$$K_2=-2+3.7028X+3.976X^2,$$
$$K_3=-2.653X-3.059X^2,$$
$$K_4=0.64178X+0.69164X^2, \tag{3.5}$$

with the expansion variable $X=1-1/N$.

The results of our theory for continuum solvents of $N=50$ are shown in Figs. 2–5 along with the SCMF calculations performed earlier by Carignano and Szleifer.[10] In these figures it can be seen that the present DFT theory is in excellent agreement with the continuum solvent simulations of Murat and Grest. As the dimensionless surface coverage $\rho_A\sigma^2$ increases from 0.01 to 0.20, both the theoretical and MD profiles become more nonparabolic and extended. Furthermore, the results of the present DFT theory are very close to those of the SCMF calculations. This is significant since the SCMF calculations were based on a SAW ideal chain model whereas, in our approach, a theory based on a random-walk, ideal chain was developed. This is of practical importance since the demands of the numerical, random-walk calculation are relatively modest, each profile typically taking only a few minutes to generate on a typical workstation.

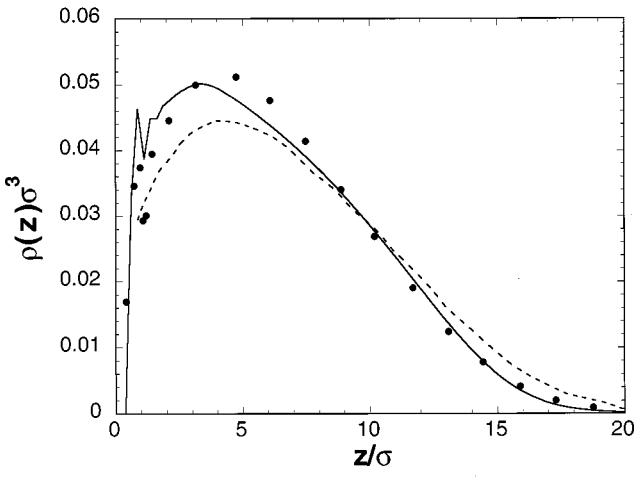

FIG. 2. Athermal, excluded volume chains of 50 sites and surface coverage of $\rho_A\sigma^2=0.01$. DFT results of current study for $\lambda\neq0$ (solid line) are compared to those of Murat and Grest (Refs. 14–18) (circles) and to those of Carignano and Szleifer (Refs. 10, 11) (dashed line).

Interestingly, the enforcement of incompressibility in our theory has very little effect on the density profile as can be seen from the insert in Fig. 4. This is certainly not the case for conventional SCF theory where the density profiles are strongly compressed by the λ-field. Both the λ and the $\hat{c}^R(0)$ contributions to the field in our incompressible DFT calculations serve to flatten and extend the density profile. Apparently, in our compressible DFT calculations the $\hat{c}^R(0)$ contribution is much stronger than that of $\lambda(z)$ making the latter term irrelevant; however, in conventional SCF theory where $\hat{c}^R(0)$ is absent, as indicated in Eq. (3.1), the more modest chain perturbation due to $\lambda(z)$ is made apparent.

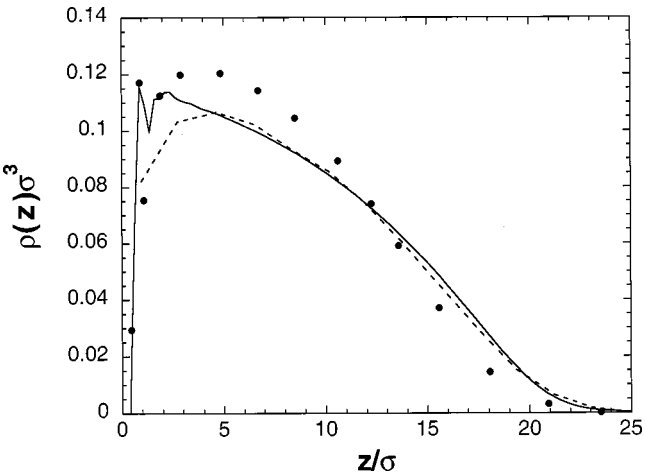

FIG. 3. Athermal, excluded volume chains of 50 sites and surface coverage of $\rho_A\sigma^2=0.03$. Symbols as in Fig. 2.

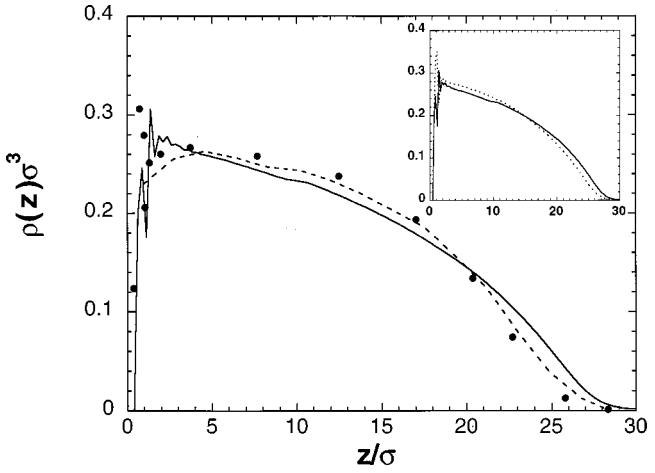

FIG. 4. Athermal, excluded volume chains of 50 sites and surface coverage of $\rho_A\sigma^2=0.1$. Symbols as in Fig. 2. The insert shows the effect of the incompressibility constraint. The solid line is the $\lambda\neq 0$ result as in the main plot while the dashed line is the $\lambda=0$ result.

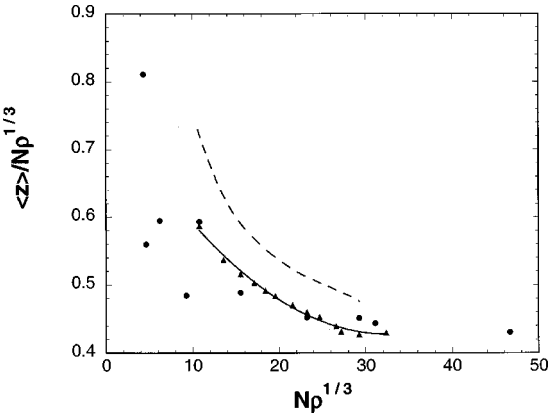

FIG. 6. Scaling of average site distance from wall for athermal, excluded volume chains. The solid line is the result of $\lambda\neq 0$, DFT for the cases of $N=50$, $\rho_A\sigma^2=0.01-0.2$ (11 points); $N=100$, $\rho_A\sigma^2=0.02$; $N=150$, $\rho_A\sigma^2=0.01$. The dashed line represents the results of Carignano and Szleifer (Refs. 10, 11). The circles are the results of Murat and Grest (Refs. 14–18).

Examination of Figs. 4 and 5 reveals that at high surface coverages, the polymer profile tends toward a step function where the polymer density is constant within the tethered layer and zero outside. Such a step profile was assumed in early scaling theories of polymer brushes.[1,2] From these scaling approaches it can be demonstrated that the layer thickness obeys the relation $\langle z\rangle\sim N\rho_A^{1/3}$ with respect to the chain length and surface coverage. A check of this prediction with our theory, along with the MD and SCMF results, is depicted in Fig. 6. It can be observed from this figure that the curves from both our theory and the Murat and Grest MD simulations, approach $\langle z\rangle\propto N\rho_A^{1/3}$ for large surface coverages and chain lengths in accordance with scaling predictions. Over this same range it appears that the SCMF results have still not reached the brushlike scaling regime.[11]

Thus far we have only considered tethered chains in a continuum solvent. We know from MD simulations[27] and PRISM theory[28] that in bulk polymer solutions, the presence of explicit solvent molecules significantly reduces the radius of gyration of the polymer compared to the continuum solvent. Thus an explicit athermal solvent is still a good solvent for the polymer, but not as good as a continuum solvent. One might expect a similar effect of explicit solvent molecules in a tethered chain system.[29] This is indeed what was observed in the MD simulations of Grest[17] who studied tethered polymers in chain solvents of various lengths. Let us consider how the fields in Eq. (2.8) are modified due to the presence of explicit solvent molecules. Now the direct correlation functions associated with the solvent are no longer zero, and, as a result, the term ξ_p no longer reduces to $\hat{c}_{pp}^R(0)$ as in Eq. (2.11) but is a balance between polymer/polymer and polymer/solvent direct correlation functions. A similar argument applies for the ξ_s term. As discussed earlier, one can argue that the various direct correlation functions balance each other so that, to first approximation, $\xi_p\cong\xi_s\cong 0$. This leads to the fields in Eqs. (2.10) or (3.1) that are commonly employed in SCF calculations, and also used in the present investigation in Fig. 1 for $N=50$.

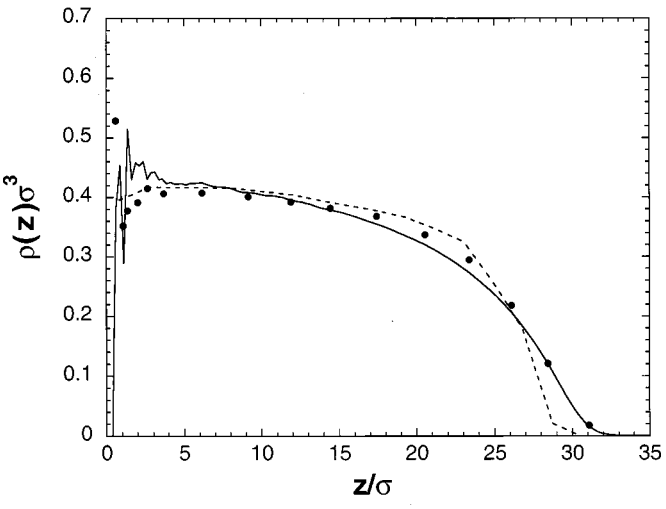

FIG. 5. Athermal, excluded volume chains of 50 sites and surface coverage of $\rho_A\sigma^2=0.2$. Symbols as in Fig. 2.

In order to compare with the athermal MD simulations of Grest[17] we performed (finite extensibility) SCF calculations on tethered chains of $N=100$ for an explicit monomeric ($N=1$) solvent using the fields in Eq. (3.1). In Figs. 7 and 8 these results are compared at two surface coverages with the corresponding tethered chains in a continuum solvent, using the fields in Eq. (3.2), along with the relevant MD simulations. Not surprisingly, the agreement between our DFT theory and simulation for the $N=100$ tethered chains in continuum solvent is excellent—just as it was for $N=50$ chains. What is remarkable, however, is that the simple SCF theory does a very good job of describing the density profiles for the tethered chains with explicit solvent molecules present. The effect of local packing can be seen in the inset. Within 6σ of the wall, the ''solvation-shell'' structure seen in high density liquids is manifest. In reality, the total density is not a constant with respect to distance from the wall, and, since the diameters of the solvent and monomer are equal in the explicit solvent simulations of Ref. 17, the layering of the total density is pronounced. Consequently,

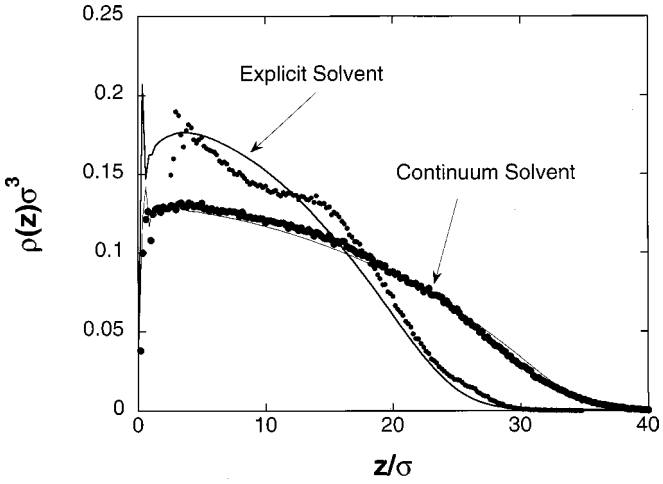

FIG. 7. Comparison of explicit and continuum solvents. The symbols are the results of computer simulation and the curves are those of DFT. The tethered chains are of length 100 and the explicit solvent is monatomic. The surface coverage is $\rho_A\sigma^2=0.03$. Near-wall simulation details are not shown.

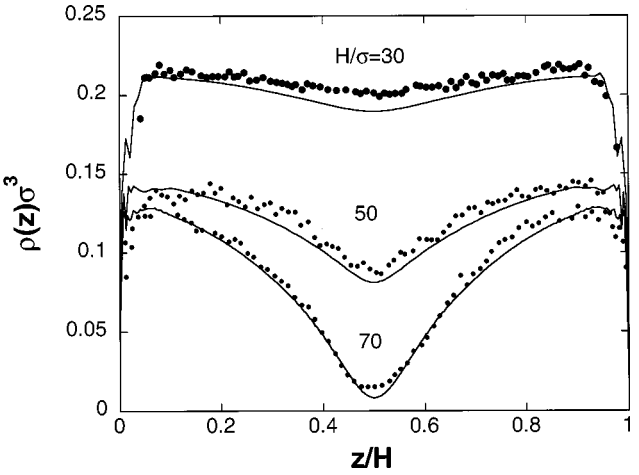

FIG. 9. Athermal (continuum-solvent) excluded volume chains of 100 sites with $\rho_A\sigma^2=0.03$ and finite wall separations, $H/\sigma=30$, 50, and 70 as indicated. The lines are the results of the DFT with $\lambda\neq 0$ and the circles are the MD results of Grest.

the structure seen in the polymer density in the six-sigma region is strongly influenced by the structure of the total density.

For walls of sufficiently small separations, the density profiles of the tethered chains on the two walls overlap. This is seen in Fig. 9, where the MD simulations of Murat and Grest[18] are well described by the DFT results. Of course, solvent effects would strongly effect the wall–wall interactions. In particular, the presence of explicit solvent would delay the overlap of the profiles until smaller wall separations. This is seen in the predictions of DFT for explicit solvents shown in Fig. 10.

IV. CONCLUSIONS

The primary intent of the current study is to formulate a general theory for tethered polymer chains based on atomic level interactions that is capable of describing both long and short range structure. We find if we sacrifice information regarding the short-range packing, then our general DFT formalism reduces to SCMF theory in the case of continuum-solvent brushes, and to SCF theory when the solvent molecule is treated explicitly. The assumptions necessary for this simplification include: locality of the fields, symmetry in the repulsive direct correlation functions, and incompressibility. By going through the DFT route, it becomes apparent that the theory can be implemented numerically through a random walk, ideal-chain model provided that the reference state is chosen appropriately. When applied to the continuum solvent problem, this approach gave results in agreement with SCMF theory and MD simulation. It should be emphasized, however, that in our formulation this agreement was achieved without resorting to a single chain Monte Carlo simulation as is required in SCMF theory.

In general, the repulsive, direct-correlation functions of polymer and solvent enter DFT theory through the fields in

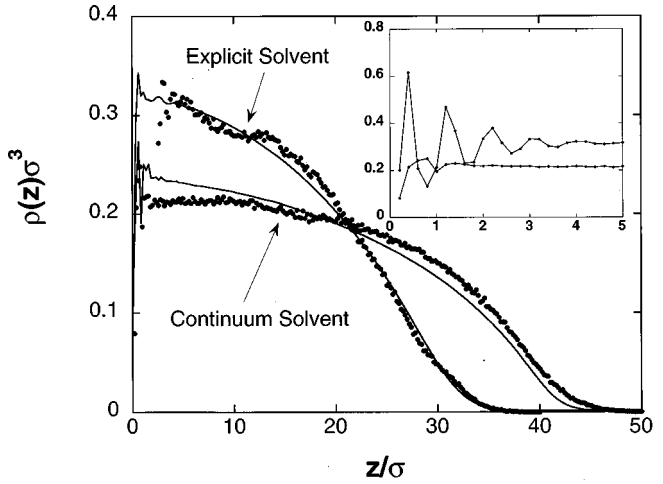

FIG. 8. Comparison of explicit and continuum solvents. Symbols as in Fig. 7 except $\rho_A\sigma^2=0.1$. Near-wall simulation details are shown in the insert, but not in the main figure.

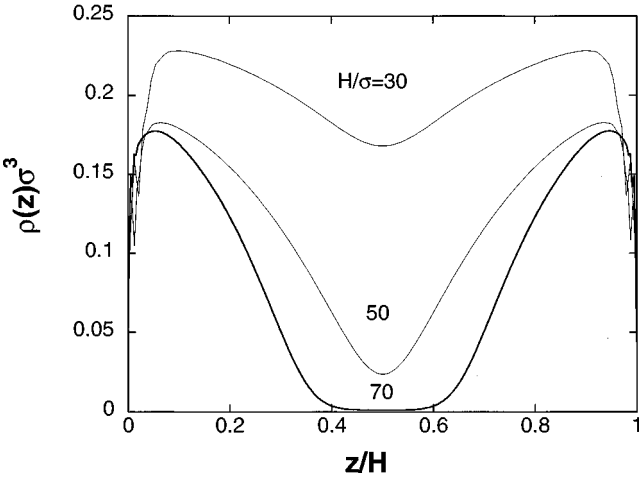

FIG. 10. Athermal, explicit-solvent, excluded-volume chains of 100 sites with $\rho_A\sigma^2=0.03$ and finite wall separations, $H/\sigma=30$, 50, and 70 as indicated. The lines are the results of the DFT with $\lambda\neq 0$.

Eq. (2.8). However, in the case of tethered, bead–spring polymers in an athermal, monatomic solvent, we found that the symmetry between the monomer and solvent structure causes the repulsive, direct-correlation functions to drop out of the problem. Beyond a distance of about six monomer diameters from the wall, the SCF-limit of the DFT theory (which includes finite extensibility) gives an accurate description of the simulations of Grest in the presence of explicit solvent molecules. In the case of more complex polymer and solvent models the specific direct correlation functions would need to be included in the calculation.

Our DFT theory, as formulated in the Appendices, is developed for a polymer model where each monomer and each solvent molecule consists of a single site. Provided there is no long range intramolecular excluded volume, the ideal polymer chain is Markovian. This permits the density profile to be calculated numerically as outlined in Appendix A. More realistic models, that faithfully reproduce monomeric and solvent architecture with multiple sites, would give a more accurate representation of the local structure. Such a model can be treated with DFT methods, however, even when the excluded volume is screened, the ideal chain is no longer Markovian. In other words, the position of the nth site on a chain will depend not just on the $(n-1)$st site, but may also on the $(n-2)$ and $(n-3)$st sites as well. It seems likely that a model, such as the ''rotational isomeric state'' model containing local architectural details, would be amenable to numerical solution if long range excluded volume effects are absent.

Throughout this work we have assumed that the various direct correlation functions are of zero range and, consequently, are proportional to delta functions. This assumption, when inserted into Eq. (2.2), leads to solvent and polymer fields that are local in the sense that the field at location z depends only on the density profile at this same location z, and not on the density at nearby locations. We expect that this locality approximation would lead to accurate predictions on long length scales, but would fail to accurately capture local packing effects near the wall. In the MD simulations of Murat and Grest, both with and without explicit solvent molecules, we see that the tethered chains do show significant local packing effects in the region within six monomer diameters of the wall. Thus the simple SCF and SCMF theories give remarkably good descriptions of tethered chains on long length scales. For many applications the near surface structure is important. For instance, the degree of solvent penetration to the wall or the pressure of a tethered chain on an opposing, bare wall would both be sensitive to the details of local packing. This is similar to the case of untethered, free polymer chains near surfaces[21–23] where the calculation of, for example, surface tension is sensitive to details of the six-sigma wall region. In order to accurately probe this wall region, DFT theory needs to be implemented with nonlocal fields incorporating the finite range of the direct correlation functions.

ACKNOWLEDGMENTS

The authors are grateful to Gary Grest for supplying previously unpublished MD results for tethered chains in explicit, monatomic solvents. J.G.C. was supported by Sandia National Laboratories, a multiprogram laboratory operated by Sandia Corporation, a Lockheed Martin Company, for the U.S. Department of Energy under Contract No. DE-AC 04-94AL 85000.

APPENDIX A: EVALUATION OF THE DENSITY PROFILE FROM THE IDEAL EXTERNAL FIELD: $\rho(z)=F[U^0(z)]$

The density profile, $\rho(z)$, of even a simple, ideal chain cannot be solved in closed form when the chain is interacting with an arbitrary external field, $U^0(z)$; however, the judicious use of Fourier transforms permits a convenient numerical solution. This approach is discussed in some generality in Ref. 21, and, in this Appendix, the specific application to tethered chains is addressed.

Of particular importance for tethered chains is the maintenance of finite extensibility. One of the primary reasons that the lattice based treatment of self-avoiding chains fails to quantitatively agree with off-lattice simulations is that the lattice chains do not rigidly enforce finite extensibility. One may also speculate that the lack of finite extensibility in the Gaussian chains used in SCF theories of tethered chains would be as large a source of error as the neglect of some of the excluded volume contributions. The approach of the current work does enforce this constraint, and, as a consequence, our results are most easily compared to those of other off-lattice studies of chains of fixed bond length.

The density distribution of a given site on an untethered chain (for instance, the 4th site of a 6 site chain) can be decomposed into the product of two integrals,

$$\rho_4(z_4)\propto I_{\text{left}}(z_4)\exp(-U^0(z_4))I_{\text{right}}(z_4), \tag{A1}$$

where

$$\begin{aligned} I_{\text{left}}(z_4)=\int\int\int \exp[-U^0(z_1)]\delta(|\underline{r}_2-\underline{r}_1|-\sigma) \\ \times\exp[-U^0(z_2)]\delta(|\underline{r}_3-\underline{r}_2|-\sigma) \\ \times\exp[-U^0(z_3)]\delta(|\underline{r}_4-\underline{r}_3|-\sigma)d\underline{r}_1d\underline{r}_2d\underline{r}_3, \end{aligned} \tag{A2}$$

and

$$\begin{aligned} I_{\text{right}}(z_4)=\int\int \delta(|\underline{r}_5-\underline{r}_4|-\sigma)\exp[-U^0(z_5)] \\ \times\delta(|\underline{r}_6-\underline{r}_5|-\sigma)\exp[-U^0(z_6)]d\underline{r}_5d\underline{r}_6, \end{aligned} \tag{A3}$$

the fields are expressed in units of k_BT; k_B is the Boltzmann constant; and T is the temperature.

Such integrals can be evaluated with Fourier transforms. Consider I_{right} as an example. Working from right to left,

$$\exp[-U^0(z_6)]=\frac{a_0}{2}+\sum_{n=1}^{\infty} a_n \cos\left(\frac{n\pi z_6}{L}\right), \tag{A4}$$

where $2L$ is the distance between the two walls of the pore; the origin of z_6 has been shifted so the function is even, and

$$a_n=\frac{1}{L}\int_{-L}^{L}\exp[-U^0(z)]\cos\left(\frac{n\pi z}{L}\right)dz. \tag{A5}$$

The right most delta function can be expressed as

$$\delta(|\underline{r}_6-\underline{r}_5|-\sigma)=\frac{1}{8\pi^3}\int_{-\infty}^{\infty}\exp[ik\cdot(\underline{r}_6-\underline{r}r_5)]\times\frac{\sin(k\sigma)}{k\sigma}d\underline{k}, \tag{A6}$$

where $i=\sqrt{-1}$. The integral over $\underline{r}_6$ is then

$$\begin{aligned}\int \delta(|\underline{r}_6-\underline{r}_5|-\sigma)\exp[-U^0(z_6)]d\underline{r}_6&=\int_{-L}^{L}\left[\frac{1}{8\pi^3}\int_{-\infty}^{\infty}\exp[i\underline{k}\cdot(\underline{r}_6-\underline{r}_5)]\frac{\sin(k\sigma)}{k\sigma}d\underline{k}\right][\exp[-U^0(z_6)]]d\underline{r}_6\\&=\frac{1}{2\pi}\int_{-\infty}^{\infty}\exp[-ik_z z_5]\frac{\sin(k_z\sigma)}{k_z\sigma}\left[\int_{-L}^{L}\exp[ik_z z_6]\exp[-U^0(z_6)]dz_6\right]dk_z\\&=\frac{1}{2\pi}\int_{-\infty}^{\infty}\exp[-k_z z_5]\frac{\sin(k_z\sigma)}{k_z\sigma}\left[\pi\sum_{n=-\infty}^{\infty}a_n\delta\left(|k_z|-\frac{n\pi}{L}\right)\right]dk_z\\&=\frac{a_0}{2}+\sum_{n=1}^{\infty}a_n\frac{\sin(n\pi\sigma/L)}{n\pi\sigma/L}\cos\left(\frac{n\pi z_5}{L}\right).\end{aligned} \tag{A7}$$

The delta function $\delta(|k_z|-n\pi/L)$ arises from treating $\exp(-U^0(z))$ as an even, periodic function from $z=-\infty$ to ∞. Only wavelengths commensurate with the function's period $(2L)$ contribute to the integral, which generates the finite Fourier transform.

The result of Eq. (A7) is a function of z_5 which is then multiplied by $\exp(-U^0(z_5))$, taken back into Fourier space to be multiplied by the next delta function, and so on until the integral is evaluated.

When starting from the tethered end, an extra site is added to Eq. (A2) and fixed to the wall with a delta function,

$$\begin{aligned}\int \delta(z_0)\delta(|\underline{r}_1-\underline{r}_0|-\sigma)d\underline{r}_0&=\int_{-L}^{L}\delta(x_0)\delta(y_0)\delta(z_0-L)\left[\frac{1}{8\pi^3}\int_{-\infty}^{\infty}\exp[i\underline{k}\cdot(\underline{r}_1-\underline{r}_0)]\frac{\sin(k\sigma)}{k\sigma}d\underline{k}\right]d\underline{r}_0\\&=\frac{1}{2\pi}\int_{-\infty}^{\infty}\exp[-ik_z r_1]\frac{\sin(k_z\sigma)}{k_z\sigma}\left[\int_{-L}^{L}\exp[-ik_z z_0]\delta(z_0-L)dz_0\right]dk_z\\&=\frac{1}{2\pi}\int_{-\infty}^{\infty}\exp[-ik_z z_1]\frac{\sin(k_z\sigma)}{k_z\sigma}\left[2\pi\sum_{n=-\infty}^{\infty}\cos(k_z L)\delta\left(|k_z|-\frac{n\pi}{L}\right)\right]dk_z\\&=1+\sum_{n=1}^{\infty}\frac{\sin(n\pi\sigma/L)}{n\pi\sigma/L}2\cos(n\pi)\cos\left(\frac{n\pi z_1}{L}\right).\end{aligned} \tag{A8}$$

Equation (A8) is a real space function which is then multiplied by $\exp(-U^0(z))$; taken into Fourier space; multiplied by $\sin(n\pi\sigma/L)/(n\pi\sigma/L)$; etc., just as for I_{right}. The product of the two integrals, I_{right} and I_{left} is multiplied by $\exp(-U^0(z))$ and normalized. For computational convenience, the trigonometric functions needed in the Fourier transforms are calculated at each k and at each real-space grid-point near the beginning of the program and stored in memory to be used during the iteration process.

Although a straightforward enough algorithm, the above is rather notationally cumbersome. As is often the case, denoting the integrals as graphs clarifies the mathematical derivations. In particular, Eq. (A1) can be rewritten as

$\rho_4(z)\propto$ 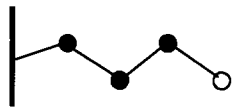 $\exp(-U^O(z))$ 

(A9)

where the black circles are $\exp(-U^0(z))$ circles which have been integrated over; the white circles are 1-circles which have not been integrated over; the thin lines are displaced delta functions, $\delta(|\underline{r}_1-\underline{r}_2|-\sigma)$; σ is the bond length; the heavy vertical line is the hard wall; and density profile of this site, $\rho_4(z)$, is normalized so that the surface coverage, ρ_A, is

$\int \rho_4(z)dz$. The total density profile {i.e., the functional $F[U^0(z)]$} is then the sum over the density profiles for each site along the chain. All of the calculations reported here were performed in slit pores of large width with identical polymer coatings on each wall.

By switching back and forth between real and Fourier space, each of the two graphs in Eq. (A9) can be found as a function of z. One of the resulting distributions will peak near the wall and have a tail extending, in this case, to a distance of 4σ. The other will peak away from the wall and have a tail towards the wall. For the case illustrated above this would not be problematic: the product of the two distributions would have a significant overlap region and, when properly normalized, $\rho_4(z)$ would result. However, if the rightmost graph in Eq. (A9) was, say, 100 sites long instead of 2, numerical problems would ensue. The right-hand distribution resulting from the procedure described above would be essentially zero over the range where the leftmost distribution is nonzero. Since the integrated value of $\rho_4(z)$ must be nonzero, the overlap of these numerically small tails must be included in the calculation.

The calculations are performed starting from the density profile of the free end, $\rho_{\text{end}}(z)$, and working in towards the sites near the tethering point. The area of each overlap region is calculated (before normalization to ρ_A). When this area drops to less than 10^{-8}, say for site i, then the density profile for site $i+1$ is used to approximate the density both for site i and for all subsequent sites. In particular, if the peak in $\rho_{i+1}(z)$ occurs at z_{i+1} and the peak in $\rho_1(z)$ is approximated as occurring at 0.25, then the peak in $\rho_j(z)$ would occur at $z_j = 0.25 + (z_{i+1} - 0.25)(j-1)/i$. Consequently, $\rho_j(z)$ was approximated as $\rho_{i+1}(0.25 + (z-0.25)i/(j-1))$ for those sites in the low overlap area [except for $\rho_1(z)$ which was taken to be a constant between the wall and its maximum extension of 0.5σ]. The grid spacing in the z-direction was 0.25σ.

Such, then, is the method we used to calculate the density profile of the polymer from the external field, and the density profile of the solvent, $\rho_s(z)$, is the comparatively trivial

$$\rho_s(z) = \rho_{s,\text{ bulk}} \exp[-U_s^0(z)], \tag{A10}$$

where $\rho_{s,\text{ bulk}}$ is the density of the solvent in the bulk which is in equilibrium with the inhomogeneous solvent; and $U_s^0(z)$ is the ideal external field of the solvent (in units of k_BT).

APPENDIX B: EVALUATION OF THE IDEAL EXTERNAL FIELD FROM THE DENSITY PROFILE: $U^0(z) = G[\rho(z)]$

Consider the energy, E, of a polymer/solvent system in the presence of external fields,

$$dE = TdS - PdV + \mu_p dn_p + \mu_s dn_s + \int_V \rho_p(r)\,\delta U_p(r)d\underline{r} + \int_V \rho_s(r)\,\delta U_s(r)d\underline{r}, \tag{B1}$$

where T is the temperature, S is the entropy, P is pressure, V is volume, μ is the chemical potential, n, is the number of sites, $\rho(r)$, is the site density, and $U(r)$ is the external field. The integrals are over the system volume; "p" denotes "polymer;" and "s" denotes solvent. The $\rho(r)$'s are constrained so that $n = \int_V \rho(r)d\underline{r}$.

From the definition $E^* = E - \int_V \rho_p(r)U_p(r)d\underline{r} - \int_V \rho_s(r)U_s(r)d\underline{r}$, one has

$$dE^* = TdS - PdV + \int_V \psi_p(r)\,\delta\rho_p(r)d\underline{r} + \int_V \psi_s(r)\,\delta\rho_s(r)d\underline{r}, \tag{B2}$$

where $\psi(r) = \mu - U(r)$. The Helmholtz free energy, A, is then $A = E^* - TS$, or

$$dA = -SdT - PdV + \int_V \psi_p(r)\,\delta\rho_p(r)d\underline{r} + \int_V \psi_s(r)\,\delta\rho_s(r)d\underline{r}. \tag{B3}$$

Finally, the grand potential free energy is $\Omega = A - \int_V \psi_p(r)\rho_p(r)d\underline{r} - \int_V \psi_s(r)\rho_s(r)d\underline{r}$, or,

$$d\Omega = -SdT - PdV - \int_V \rho_p(r)\,\delta\psi_p(r)d\underline{r} - \int_V \rho_s(r)\,\delta\psi_s(r)d\underline{r}. \tag{B4}$$

At fixed T, V, and $\rho(r)$'s, Ω will be minimized. If constraints are added to the system to force the densities away from equilibrium, the resulting grand potential free energy, denoted $W[\rho_p(r),\rho_s(r)]$, will be greater that Ω, and

$$\Omega = \min_{\rho_p(r),\rho_s(r)} W[\rho_p(r),\rho_s(r)]. \tag{B5}$$

The heart of DFT theory (and, by extension, SCF theory) is the development of an expression for the functional $W[\rho_p(r),\rho_s(r)]$ which is then minimized with respect to $\rho_p(r)$ and $\rho_s(r)$. These density profiles which minimize the free energy functional are the equilibrium densities and the value of $W[\cdots]$ at the minimum is Ω. The only approximations in such an approach are those associated with the form of $W[\cdots]$.

A straightforward approach to developing an approximation for $W[\cdots]$ employs a functional Taylor series of the Helmholtz free energy in terms of the densities and at constant volume and temperature,

$$A = A_{\text{ref}} + \int_V \psi_{s,\text{ref}}\Delta\rho_s(r)d\underline{r} + \int_V \psi_{p,\text{ref}}\Delta\rho_p(r)d\underline{r} + \tfrac{1}{2}\int_V\int (A''_{pp}(r-r')\Delta\rho_p(r)\Delta\rho_p(r') + 2A''_{ps}(r-r')\Delta\rho_p(r)\Delta\rho_s(r') + A''_{ss}(r-r')\Delta\rho_s(r)\Delta\rho_s(r'))d\underline{r}d\underline{r}', \tag{B6}$$

where "ref" denotes the homogeneous, reference liquid about which the expansion is performed; $\Delta\rho(r) = \rho(r)$

$-\rho_{\mathrm{ref}}$; and A'' is the second functional derivative of A with respect to the indicated $\rho(r)$'s. Since $A'=\psi$, then $A''=\delta\psi/\delta\rho$ and since $\delta\rho/\delta\psi=\rho\omega(r-r')+\rho\rho h(r-r')$, a definition of the direct correlation function, $c(r)$, as $\delta\psi/\delta\rho=\omega^{-1}(r-r')/\rho-c(r-r')$ is consistent with liquid state theory. Here ω^{-1} is the functional inverse of the single chain correlation function for the *PP* case, is 0 for the *PS* case, and is $\delta(r-r')$ for the *SS* case. The pair correlation function, $g(r)$, is $h(r)+1$. In particular,

$$A''_{pp}(r-r')=\frac{\omega^{-1}(r-r')}{\rho_p}-c_{pp}(r-r'),$$

$$A''_{ps}(r-r')=-c_{ps}(r-r'), \tag{B7}$$

$$A''_{ss}(r-r')=\frac{\delta(r-r')}{\rho_s}-c_{ss}(r-r').$$

Higher order terms in Eq. (B6) are important, and, in order to correct for these terms, the free energy of an "ideal" system, denoted by "0," is also expanded and the difference taken with Eq. (B6). This yields

$$(A-A^0)=(A_{\mathrm{ref}}-A^0_{\mathrm{ref}})+\sum_{i=s,p}\int_V(\psi_{i,\mathrm{ref}}-\psi^0_{i,\mathrm{ref}})\Delta\rho_i(r)d\underline{r}-\frac{1}{2}\sum_{i,j=s,p}\int\int_V c_{i,j}(r-r')\Delta\rho_i(r)\Delta\rho_j(r')d\underline{r}d\underline{r}'$$

$$+\frac{1}{2}\int\int_B\frac{(\omega^{-1}(r-r')-\omega_0^{-1}(r-r'))}{\rho_{p,\mathrm{ref}}}\Delta\rho_p(r)\Delta\rho_p(r')d\underline{r}d\underline{r}', \tag{B8}$$

and the fundamental approximation in DFT theory is that the higher order terms have been negated by taking this difference. Of course, since the ideal and reference systems have been loosely defined at this point, it is difficult to evaluate the accuracy of this approximation; in particular, the "closer" the ideal system is to the fully interacting system, the better the approximation. We have allowed for a difference in ω^{-1} for the real and ideal systems; however, as long as the real and ideal chains are of equal length, the integrated values of the two ω^{-1} will be equal to 1/(chain length).

The Helmholtz free energies in Eq. (B8) can now be changed to $W[\cdots]$'s,

$$\Delta W=\Delta W^0-\sum_{i=s,p}\int_V(\psi_i(r)-\psi_{i,\mathrm{ref}})\rho_i(r)d\underline{r}+\sum_{i=s,p}\int_V(\psi^0_i(r)-\psi^0_{i,\mathrm{ref}})\rho_i(r)d\underline{r}-\frac{1}{2}\sum_{i,j=s,p}\int\int_V c_{i,j}(r-r')$$

$$\times\Delta\rho_i(r)\Delta\rho_j(r')d\underline{r}d\underline{r}'+\frac{1}{2}\int\int_V\frac{(\omega^{-1}(r-r')-\omega_0^{-1}(r-r'))}{\rho_{p,\mathrm{ref}}}\Delta\rho_p(r)\Delta\rho_p(r')d\underline{r}d\underline{r}', \tag{B9}$$

where $\Delta W=W-W_{\mathrm{ref}}$. In order to minimize W (or, equivalently, ΔW) with respect to $\rho(r)$, the ideal system must be evaluated.

The ideal system we consider here is that of freely jointed chains and a point particle solvent. The density profiles can be related to W^0 through Eq. (B4) where it is indicated that $\delta W/\delta\psi=\rho$. From the generalization of Eq. (A1), it can be shown that

$$W^0=\int\cdots\int\exp\left(\sum_{i=1}^N\psi^0_p(r_i)\right)S(\underline{r}_1\cdots\underline{r}_N)d\underline{r}_1\cdots d\underline{r}_N$$

$$+\int\exp(\psi^0_s(r))d\underline{r}, \tag{B10}$$

where N is the number of sites on a chain and $S(\cdots)$ is the product of delta functions which enforces the bonding constraints. The ideal chemical potentials, μ^0, are defined so that $N\mu^0_p=\ln(\rho_p)$ and $\mu^0_s=\ln(\rho_s)$.

In general, the $\psi^0(r)$'s cannot be expressed as a functional of the $\rho(r)$'s, and, as a result, the minimization of ΔW must be performed as a constrained minimization. This is done through the equations $\delta W/\delta\psi^0=0$ and $\delta W/\delta\rho=0$ where the expression (B10) is used for W^0. The former of these yields $\rho(r)=F[U^0(r)]$ which was the subject of Appendix A, and the latter yields

$$U^0_p(r)=U_p(r)-\sum_{i=s,p}\int c_{p,j}(r-r')\Delta\rho_i(r')d\underline{r}'$$

$$+\int\frac{(\omega^{-1}(r-r')-\omega_0^{-1}(r-r'))}{\rho_{p,\mathrm{ref}}}\Delta\rho_p(r')d\underline{r}',$$

$$U^0_s(r)=U_s(r)-\sum_{i=s,p}\int c_{s,j}(r-r')\Delta\rho_i(r')d\underline{r}', \tag{B11}$$

where constant terms have been dropped. This equation is reasonably general; neither the ideal nor the reference system is specified. In the body of the paper it is used as a starting point for the analysis of tethered chains.

[1] S. Alexander, J. Phys. (Paris) **38**, 983 (1977).
[2] P. G. de Gennes, Macromolecules **13**, 1069 (1980).
[3] J. M. H. M. Scheutjens and G. J. Fleer, J. Phys. Chem. **83**, 1619 (1979).
[4] T. Cosgrove, T. Heath, B. van Lent, and J. M. H. M. Scheutjens, Macromolecules **20**, 1692 (1987).
[5] K. R. Shull, J. Chem. Phys. **94**, 5723 (1991).
[6] R. Baranowski and M. D. Whitmore, J. Chem. Phys. **108**, 9885 (1998).
[7] M. Laradji, H. Guo, and M. J. Zuckermann, Phys. Rev. E **49**, 3199 (1994).
[8] J. I. Martin and Z. G. Wang, J. Phys. Chem. **99**, 2833 (1995).
[9] S. T. Milner, J. Chem. Soc., Faraday Trans. **86**, 1349 (1990); S. T. Miller, T. A. Witten, and M. E. Cates, Macromolecules **21**, 2610 (1988).
[10] M. A. Carignano and I. Szleifer, J. Chem. Phys. **98**, 5006 (1993).
[11] I. Szleifer and M. A. Carignano, Adv. Chem. Phys. **94**, 165 (1995); I. Szleifer and M. A. Carignano, Macromol. Rapid Commun. **21**, 423 (2000).
[12] S. T. Milner, Science **251**, 905 (1991).
[13] A. Halperin, M. Tirrell, and T. P. Lodge, Adv. Polym. Sci. **100**, 31 (1991).
[14] G. S. Grest and M. Murat, in *Monte Carlo and Molecular Dynamics Simulations in Polymer Science*, edited by K. Binder (Oxford University Press, New York, 1995), p. 476.
[15] M. Murat and G. S. Grest, Macromolecules **22**, 4054 (1989).
[16] G. S. Grest and M. Murat, Macromolecules **26**, 3108 (1993).
[17] G. S. Grest, J. Chem. Phys. **105**, 5532 (1996).
[18] M. Murat and G. S. Grest, Phys. Rev. Lett. **63**, 1074 (1989); G. S. Grest (private communication).
[19] P. Y. Lai and K. Binder, Makromol. Chem., Macromol. Symp. **65**, 189 (1993), and references therein.
[20] D. Chandler, J. D. McCoy, and S. J. Singer, J. Chem. Phys. **85**, 5971 (1986).
[21] J. D. McCoy, M. A. Teixeira, and J. D. Curro, J. Chem. Phys. **114**, 4289 (2001).
[22] S. K. Nath, J. D. McCoy, J. G. Curro, and R. S. Saunders, J. Polym. Sci., Part B: Polym. Phys. **33**, 2307 (1995); J. Chem. Phys. **106**, 1950 (1997); **108**, 3023 (1998).
[23] J. B. Hooper, J. D. McCoy, and J. G. Curro, J. Chem. Phys. **112**, 3090 (2000); J. B. Hooper, M. T. Pileggi, J. D. McCoy, J. G. Curro, and J. D. Weinhold, *ibid.* **112**, 3094 (2000); J. B. Hooper, J. D. McCoy, J. G. Curro, and F. van Swol, *ibid.* **113**, 2021 (2000).
[24] A. Yethiraj and C. E. Woodward, J. Chem. Phys. **102**, 5499 (1995).
[25] K. Huang and A. C. Balazs, Macromolecules **26**, 1914 (1993).
[26] W. W. Graessley, R. C. Hayward, and G. S. Grest, Macromolecules **32**, 3510 (1999).
[27] S. Mendez, J. G. Curro, M. Puetz, D. Bedrov, and G. D. Smith, J. Chem. Phys. **115**, 5669 (2001).
[28] N. F. Carnahan and K. E. Starling, J. Chem. Phys. **51**, 635 (1969); D. J. Tildesley and W. B. Street, Mol. Phys. **41**, 341 (1980); J. Chang and S. I. Sandler, Chem. Eng. Sci. **49**, 2777 (1994); F. A. Escobedo and J. J. de-Pablo, J. Chem. Phys. **102**, 2636 (1995).
[29] M. Aubouy, G. H. Fredrickson, P. Pincus, and E. Raphael, Macromolecules **28**, 2979 (1995).